Influence of Wake Models on Calculated Tiltrotor Aerodynamics

Wayne Johnson

Army/NASA Rotorcraft Division
NASA Ames Research Center
Moffett Field, California

Comparisons of measured and calculated aerodynamic behavior of a tiltrotor model are presented. The test of the Tilt Rotor Aeroacoustic Model (TRAM) with a single, 1/4-scale V-22 rotor in the German-Dutch Wind Tunnel (DNW) provides an extensive set of aeroacoustic, performance, and structural loads data. The calculations were performed using the rotorcraft comprehensive analysis CAMRAD II. Presented are comparisons of measured and calculated performance and airloads for helicopter mode operation, as well as calculated induced and profile power and wake geometry. The focus of this paper is on the further development of wake models for tiltrotors in helicopter mode operation. Three tiltrotor wake models are considered, characterized as the rolled-up, multiple-trailer, and multiple-trailer with consolidation models. By using a free wake geometry calculation method that combines the multiple-trailer wake model with a simulation of the tip vortex formation process (consolidation), good correlation of the calculations with TRAM measurements is obtained for both performance and for airloads.

Notation·

a	speed of sound
A	rotor disk area, πR^2
c_n	blade section normal force coefficient, $N/(\frac{1}{2}\rho U^2 c)$
c_{ref}	blade reference chord
C_P	rotor power coefficient, $P/\rho(\Omega R)^3 A = Q/\rho(\Omega R)^2 RA$
C_T	rotor thrust coefficient, $T/\rho(\Omega R)^2 A$ (shaft axes)
C_X	rotor propulsive force coefficient, $X/\rho(\Omega R)^2 A$ (wind axes, positive forward)
G	strength of trailed vorticity
$M^2 c_n$	blade section normal force coefficient times Mach number squared, $N/(\frac{1}{2}\rho a^2 c)$
M_{tip}	blade tip Mach number, $\Omega R/a$
N	number of blades
N	blade section normal force
r	blade radial station (0 to R)
r_c	vortex core radius
r_C	centroid of vorticity
r_G	moment (radius of gyration) of vorticity
R	blade radius
P	rotor power, $P = \Omega Q$
q	dynamic pressure, $\frac{1}{2}\rho V^2$
Q	rotor torque
T	rotor thrust (shaft axes)
X	rotor propulsive force (wind axes, positive forward)
V	wind tunnel speed
α, α_s	rotor shaft angle (positive aft, zero for helicopter mode)
μ	advance ratio, $V/\Omega R$
ρ	air density
σ	rotor solidity, $Nc_{ref}/\pi R$ ($\sigma = 0.105$ for TRAM)
ψ	blade azimuth angle (zero azimuth is downstream)
Ω	rotor rotational speed

·*Presented at the American Helicopter Society Aerodynamics, Acoustics, and Test and Evaluation Technical Specialists Meeting, San Francisco, CA, January 23-25, 2002.*

Introduction

The tiltrotor aircraft configuration has the potential to revolutionize air transportation by providing an economical combination of vertical take-off and landing capability with efficient, high-speed cruise flight. To achieve this potential it is necessary to have validated analytical tools that will support future tiltrotor aircraft development. These analytical tools must calculate tiltrotor aeromechanical behavior, including performance, structural loads, vibration, and aeroelastic stability, with an accuracy established by correlation with measured tiltrotor data. For many years such correlation has been performed for helicopter rotors (rotors designed for edgewise flight), but correlation activities for tiltrotors have been limited, in part by the absence of appropriate measured data. The test of the Tilt Rotor Aeroacoustic Model (TRAM) with a single, 1/4-scale V-22 rotor in the German-Dutch Wind Tunnel (DNW) now provides an extensive set of aeroacoustic, performance, and structural loads data.

An investigation is being conducted to calculate tiltrotor aeromechanics behavior using CAMRAD II, and compare the results with the TRAM DNW measured data. CAMRAD II is a modern rotorcraft comprehensive analysis, with advanced models intended for application to tiltrotor aircraft as well as helicopters. The objectives of this investigation are to establish the level of predictive capability achievable with current technology; identify the limitations of the current aerodynamic and wake models of tiltrotors; and produce recommendations for research to extend tiltrotor aeromechanics analysis capability.

Previous papers from this investigation (refs. 1 and 2) have described an aerodynamic and wake model and calculation procedure that reflects the unique geometry and phenomena of tiltrotors. In particular, the tiltrotor model includes stall delay for inboard blade sections. The work included application of two wake models (described below), both different from the wake models that have been successfully used with helicopter rotors. It was found (ref. 2) that one of these tiltrotor wake models was best for performance calculations, and the other was best for airloads calculations.

The present paper focuses on the further development of wake models for tiltrotors in helicopter mode operation. Results are presented for performance, airloads, and wake geometry calculations, compared with TRAM DNW measurements.

TRAM DNW Test

The purpose of the Tilt Rotor Aeroacoustic Model (TRAM) experimental project is to provide the data necessary to validate tiltrotor performance and aeroacoustic prediction methodologies and to investigate and demonstrate advanced civil tiltrotor technologies.

In April-May 1998 the TRAM was tested in the isolated rotor configuration at the Large Low-speed Facility of the German-Dutch Wind Tunnels (DNW). A preparatory test was conducted in December 1997. These tests were the first comprehensive aeroacoustic tests for a tiltrotor, including not only noise, performance, and structural loads data, but airload and wake measurements as well. The TRAM and the DNW test are described in references 3 to 6. Figure 1 shows the wind tunnel installation of the TRAM isolated rotor. The LLF/DNW is a closed return, atmospheric pressure wind tunnel. The TRAM test utilized the 6- by 8-meter open-jet test section, which is in a large anechoic testing hall.

The Tilt Rotor Aeroacoustic Model (TRAM) is a general-purpose test bed for moderate-scale tiltrotor models. TRAM consists of two hardware-interchangeable test rigs: an isolated rotor test stand, and a full-span, dual-rotor model. The contractor team of MicroCraft and McDonnell Douglas Helicopter (now Boeing) had overall responsibility for the TRAM development, under the direction of the Aeromechanics Branch, Army/NASA Rotorcraft Division, NASA Ames Research Center.

TRAM Physical Description

The TRAM was designed as a 1/4-scale V-22 tiltrotor aircraft model. The rotor has a diameter of 9.5 ft. The rotor was tested at a tip Mach number of 0.63 in helicopter mode (because of operational limitations, this was lower than the V-22 tip Mach number of 0.71); and 0.59 in airplane mode (matching the V-22). The rotor and nacelle assembly was attached to an acoustically-treated, isolated rotor test stand through a mechanical pivot (the nacelle conversion axis), as shown in figure 1. The nacelle (but not the spinner) contours model the V-22. The test stand contained the electric motor assembly, and was attached to the DNW sting mount. The conversion angle was manually adjusted, set to 90 deg nacelle angle for helicopter mode and 0 deg nacelle angle for airplane mode testing.

Reference 7 provides complete details of the TRAM physical description. Table 1 presents the principal characteristics of the TRAM. The solidity $\sigma = 0.105$ is the official value (thrust-weighted), used to normalize measured and calculated data in this report. Figure 2 shows the blade chord and twist distributions. The TRAM blade airfoils are the V-22 airfoils designated XN28, XN18, XN12, XN09, at radial stations r/R = 0.2544, 0.50, 0.75, 1.00 respectively. The root fairing has a special airfoil section. The airfoil tables used in the present investigation are those generated during the JVX program in the mid 1980's. Reference 8 is the source of the airfoil data. The data are from pressure wind tunnel tests of 6.5 inch chord airfoils, at Reynolds number

Figure 1. Tilt Rotor Aeroacoustic Model in the German-Dutch Wind Tunnel (TRAM DNW).

Table 1. Principal physical characteristics of the TRAM model.

gimballed hub, trailing pitch link	
blade radius R	4.75ft = 1.45m
solidity σ (thrust weighted)	0.105
number of blades	3
design rotor speed, helicopter	M_{tip} = 0.708
design rotor, airplane	M_{tip} = 0.593
airfoil sections	XN28, XN18, XN12, XN09
precone	2 deg
nominal pitch flap coupling, δ_3	–15 deg

of approximately Re/M = 15 to 20 million (M is the Mach number). For the root fairing the V-22 cuff airfoil data were used, although the contours of the TRAM root fairing do not match the V-22 because of constraints imposed by the blade pitch case geometry and construction.

The rotor blades and hub are designed as geometrically and dynamically scaled models of the V-22 blades. The hub is gimbaled with a constant velocity joint consisting of a spherical bearing and elastomeric torque links. The balance and flex-coupling measure forces and torque. The blade set has both strain-gauged and pressure-instrumented blades. There are 150 pressure transducers distributed over two blades: primarily at radial stations 0.50, 0.62, 0.82, and 0.96 on blade #1, and at radial stations 0.33, 0.72, 0.90, and 0.98 on blade #2. At the start of the test, 135 of the pressure gages were operational. These pressure measurements can be integrated chordwise to obtain blade section normal force at seven radial stations (there are too few chordwise points at 98% radius to get section normal force). Reference 5

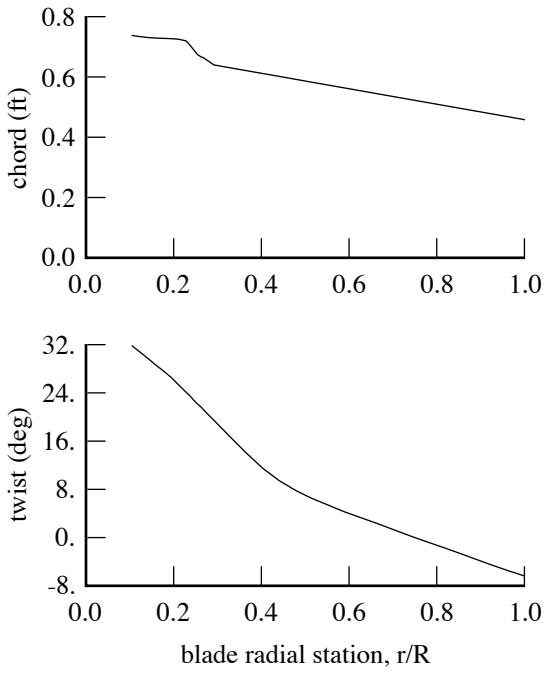

Figure 2. TRAM chord and twist distributions.

describes the data reduction process for the blade pressures and section normal force. The third blade carries all of the required safety of flight strain gauge instrumentation.

Data Reduction and Corrections

All measured quantities were sampled at 64 per-rev, except for the pressure and acoustic measurements, which were sampled at 2048 per-rev. Data were collected for 64 revolutions. The results in this report are a single revolution of data obtained by averaging over the 64 revolutions collected. To eliminate high frequency noise, the airloads data are harmonically analyzed, and 64 harmonics are used to reconstruct the time history at 256 points in a revolution (reduced from 1024 harmonics representing 2048 samples). All the blade-vortex interaction events in the section normal force data are captured using 64 harmonics.

The measured balance loads of the TRAM in the DNW are corrected for the influence of the wind tunnel walls, by using the corrected shaft angle of attack and wind axis propulsive force. Reference 1 describes the wind tunnel wall correction in more detail, and shows the influence of this correction on the performance correlation.

Aerodynamic tares are subtracted from the measured rotor forces and torque. For helicopter mode, the blades were removed but the root fairings around the pitch cases were retained; and the ends of the root fairings were sealed with foam inserts. These tare corrections remove the effects of

gravity, the spinner, and (for helicopter mode) the blade root fairings from the measured performance data. The calculated performance (forces and power) does not include the blade weight, and the analysis does not model the spinner. The analysis does include the root fairing, so for helicopter mode it is necessary to apply a tare correction to the calculated performance. With these tare corrections, the measured and calculated performance data can be directly compared. The calculations must include the root fairing, since the root fairing does influence the wake and the loading on the rest of the blade. Reference 1 describes the analysis tare correction in more detail, and shows the influence of this correction on the performance correlation.

The data reduction process for the pressure and airloads measurements is described in reference 5. The pressure coefficient is obtained from the pressure by dividing by the local section dynamic pressure: $c_p = p/(\frac{1}{2}\rho U^2)$. It follows that the section normal force coefficient, obtained by integrating the pressure coefficients, is $c_n = N/(\frac{1}{2}\rho U^2 c)$; where c is the local chord. Since the operating conditions of interest in this report do not involve significant stall at the measurement locations, it is more interesting to look at the quantity $M^2 c_n = N/(\frac{1}{2}\rho a^2 c)$, where M=U/a is the section Mach number. The section airloads can be integrated to obtain the rotor thrust. A comparison of the rotor thrust measured by the balance with the rotor thrust obtained by integrating the blade pressure measurements shows that the thrust from the airloads is consistently lower than the thrust from the balance, by 15 to 19%. The balance measurement of rotor thrust is considered accurate. The cause of this difference is not known. Examination of the chordwise pressure distributions at the seven radial stations does not suggest any problem.

DNW Test Results

The operating conditions of the TRAM in the DNW covered helicopter mode, airplane mode, and hover. The rotor shaft angle of attack is positive aft, around zero (–14 to +14 deg) for helicopter mode and around –90 deg for airplane mode. The tip Mach number M_{tip} is the ratio of the rotor tip speed to the speed of sound. The advance ratio μ is the ratio of the tunnel speed to the rotor tip speed, regardless of the shaft angle. The helicopter mode test points are for nominal advance ratios of μ = 0.125, 0.150, 0.175, 0.200; nominal thrust coefficients of C_T = 0.009, 0.011, 0.013; at shaft angles from –14 deg to 12 deg. Reference 1 provides further details of the TRAM test results from the DNW.

The TRAM helicopter mode performance measured in the DNW is shown in figure 3, in terms of rotor power and propulsive force as a function shaft angle of attack for two rotor thrust values and four advance ratios. It is also useful to examine the rotor equivalent drag:

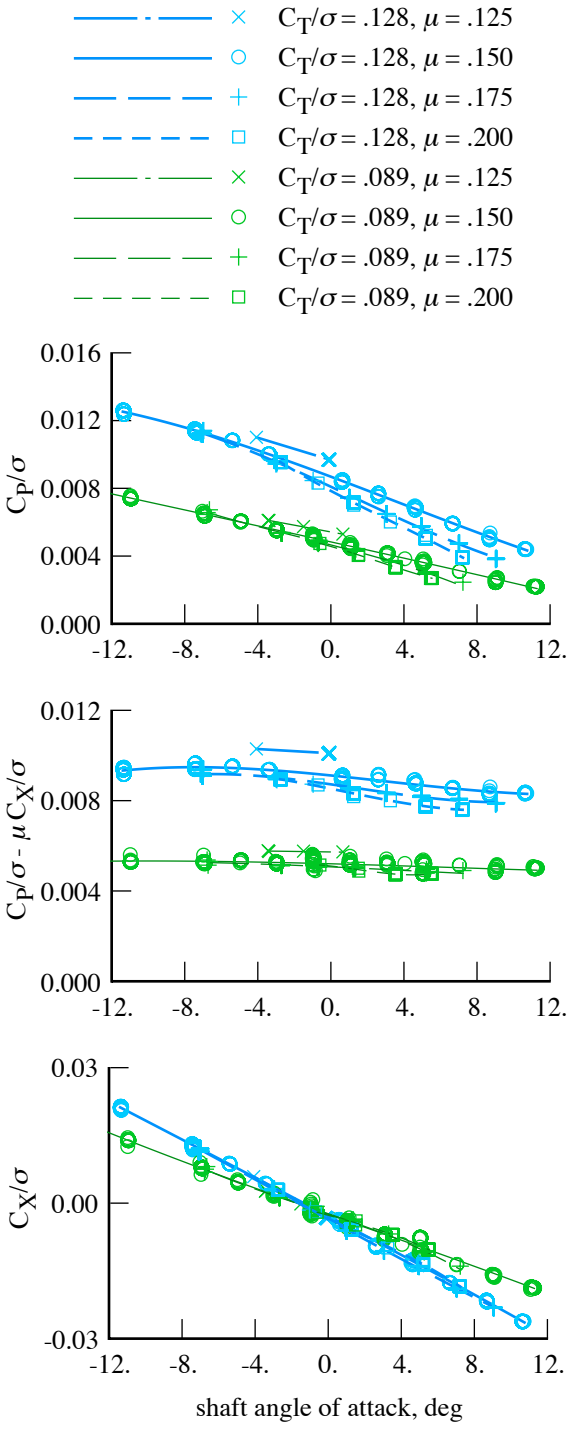

Figure 3. Measured TRAM helicopter mode performance.

$$\mu C_{De} = C_P - \mu C_X = C_{Pi} + C_{Po}$$

By definition, μC_X is the rotor parasite power, so μC_{De} is the sum of the induced and profile power. Most of the reduction of power as angle of attack increases is accounted for by the parasite power (μC_X), but the equivalent drag still shows a decrease with angle of attack, indicating that the tiltrotor (like the helicopter rotor) becomes more efficient as the propulsive force is reduced. The power increases with thrust, and decreases with advance ratio, as expected at low speed. Most of the variation of the propulsive force with shaft angle of attack and thrust is accounted for by the tilt of the thrust vector with the shaft (αC_T), so the shaft-axis inplane force is a relatively constant drag value.

For detailed examination of the airloads in helicopter mode forward flight, twelve points were selected. The nominal operating conditions are advance ratio $V/\Omega R$ = 0.15, rotor thrust C_T/σ = 0.089 and 0.128, shaft angle of attack from –10 deg (forward) to +10 deg (aft). Table 2 gives the details of the measured operating condition for these twelve points. The corrected shaft angle of attack includes the effect of the wind tunnel walls; the rotor propulsive force C_X/σ is the corrected value. The azimuth correction $\Delta\psi$ accounts for the torque link deflection. The gimbal tilt is obtained from the first harmonics of the measured gimbal deflection. The longitudinal gimbal tilt β_{1c} is positive forward; the lateral gimbal tilt β_{1s} is positive towards the advancing side.

The blade section airloads measured in helicopter mode are presented in figure 4. The figure shows M^2c_n as a function of azimuth, at one of the seven radial stations (r = 0.90R). For each of the twelve operating conditions examined, airloads data are available for several repeat points (at least three points, as many as eight points). The airloads data from different points at the same operating condition exhibit little difference. The measured airloads show significant blade-vortex interaction at the tip for all twelve conditions, at both high and low thrust, and at both positive and negative shaft angles. There is a substantial region of negative loading on the advancing blade tip, extending inboard of 0.90R at low thrust and inboard of 0.96R at high thrust and aft shaft tilt angles.

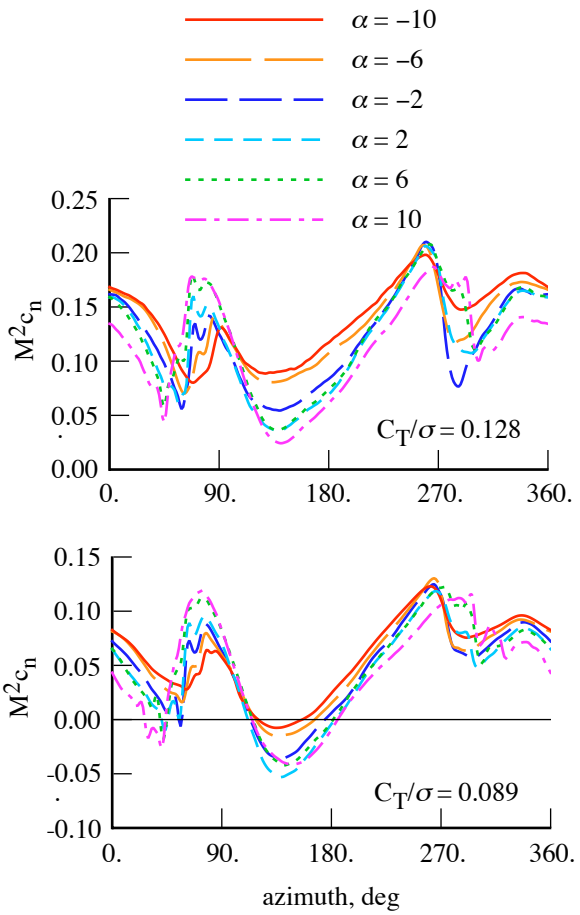

Figure 4. Measured TRAM helicopter mode airloads for μ = 0.15, at radial station r = 0.90R.

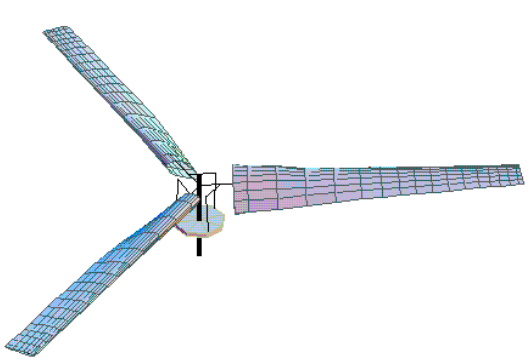

Figure 5. CAMRAD II model of TRAM.

Rotorcraft Analysis

The TRAM was analyzed using the rotorcraft comprehensive analysis CAMRAD II. CAMRAD II is an aeromechanical analysis of helicopters and rotorcraft that incorporates a combination of advanced technologies, including multibody dynamics, nonlinear finite elements, and rotorcraft aerodynamics. The trim task finds the equilibrium solution (constant or periodic) for a steady state operating condition, in this case a rotor operating in a wind tunnel. For wind tunnel operation, the thrust and flapping

(longitudinal and lateral gimbal tilt) are trimmed to target values. The aerodynamic model includes a wake analysis to calculate the rotor nonuniform induced-velocities, using free wake geometry. CAMRAD II is described in references 9 to 13.

Figure 5 illustrates the CAMRAD II model of the TRAM. The analytical model has a fixed shaft (no test stand dynamics) and constant rotor rotational speed (no drive train dynamics). The hub has a gimbal joint at the center of rotation, with nominal pitch/gimbal coupling of $\delta_3 = -15$ deg. Additional details of the model are given in reference 1. The CAMRAD II solution for the periodic rotor motion in trim used 10 harmonics of 12 cantilever elastic blade modes plus the gimbal degree of freedom.

The aerodynamic model uses lifting-line theory with a vortex wake calculation of the induced velocity. The blade aerodynamic surfaces are represented by 16 panels, from the root cutout of r/R = 0.10558 to the tip, with panel widths varying from 0.09R inboard to 0.025R at the tip. Midpoints of seven of the aerodynamic panels are aligned with the pressure instrumentation on the TRAM blades, to avoid additional interpolation in the comparison of calculated and measured airloads. The drag coefficients in the airfoil tables are corrected to the lower Reynolds number of the 1/4-scale model, using a factor equal to the Reynolds number ratio to the 1/5-power.

There is evidence that rotational effects on the boundary layer produce a delay of separation on rotor blades, particularly for the inboard sections of tiltrotors and wind turbines (refs. 14 and 15). This stall delay is modelled using input factors K_{sd} to modify the lift and drag coefficients obtained from the airfoil tables:

$$c_l = c_{l\ table} + K_{sdL}\left(c_{l\alpha}(\alpha - \alpha_z) - c_{l\ table}\right)$$

$$c_d = c_{d\ table} + K_{sdD}\left(c_{dz} - c_{d\ table}\right)$$

where $c_{l\alpha}$ is the lift-curve slope, and α_z and c_{dz} are the angle of attack and drag coefficient at zero lift. The equations given by Selig (ref. 15) are used to evaluate the stall delay factors, which depend on the blade chord distribution. The values of K_{sd} used in the TRAM analysis are shown in figure 6.

The influence of the aerodynamic model on the calculated TRAM helicopter mode performance for $\mu = 0.15$ is illustrated in figure 7. Without the Reynolds number correction of the drag from the airfoil tables, the calculated power is too low. Without the stall delay model, particularly for the lift, the calculated power is much too high, especially at the higher thrust. The stall delay model is required for accurate calculation of the tiltrotor performance in helicopter mode forward flight. The stall delay model is discussed in more detail in reference 2. The focus of the present paper is on the wake model, but it is important to remember the relative influence of the aerodynamic model features.

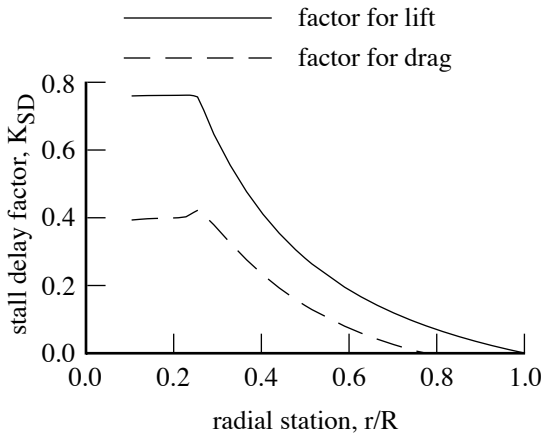

Figure 6. Stall delay factor for TRAM blade.

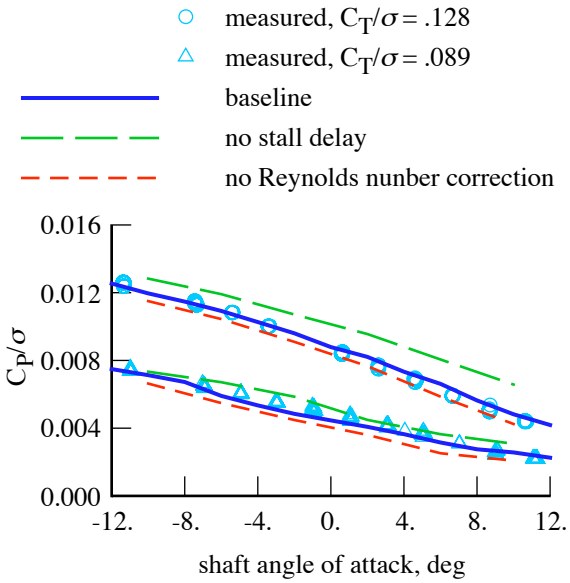

Figure 7. Influence of aerodynamic model on calculated TRAM helicopter mode performance ($\mu = 0.15$).

The calculations were performed for specified advance ratio (V/ΩR), tip Mach number, and shaft angle of attack. The analysis trim loop adjusts collective and cyclic to achieve target values of the rotor thrust (C_T/σ) and mean gimbal tilt. The shaft angle of attack values in the analysis correspond to the measured values with wind tunnel wall corrections applied. For comparison of trends with operating condition, involving many measured points, the target thrust is a nominal value and the target gimbal tilt is zero. For comparison with specific data points, the measured thrust

and measured one per-rev gimbal tilt are the target trim values for the analysis. Similarly, for trends the operating condition is defined by nominal values of advance ratio, tip Mach number, shaft angle of attack, air density, and temperature; while for specific data points the measured values are used.

In the calculations it is possible to separately evaluate the induced power and the profile power. The induced power can be presented as the ratio $\kappa = C_{Pi}/C_{Pideal}$, where C_{Pideal} is the ideal power obtained from momentum theory. The profile power can be presented as an equivalent blade drag coefficient, $c_{do} = 8C_{Po}/\sigma$.

Tiltrotor Wake Models

The CAMRAD II rotor wake analysis uses second-order lifting line theory, with the general free wake geometry calculation described in references 12 and 13. Two tiltrotor wake models are described in references 1 and 2, characterized as the rolled-up and the multiple-trailer models. Figures 8 and 9 illustrate the wake geometry for these two models. The blades are at azimuth angles of 45, 165, and 285 deg; the operating condition is $\mu = 0.15$, $\alpha_s = 6$, $C_T/\sigma = 0.089$.

The rolled-up wake model for tiltrotors (figure 8) evolved as follows from the typical helicopter wake model, based on correlation with the TRAM DNW performance measurements. For helicopter mode operation (edgewise flight at moderate speed, $\mu = 0.125$ to 0.200), the high twist of the tiltrotor blades results in negative tip loading over most of the advancing side. Hence the dual-peak model must be used, in which the tip vortex is defined by the negative tip loading (not by the maximum positive bound circulation on the inboard part of the blade). A core radius of 20% mean chord is used for the tip vortex. The positive trailed vorticity inboard of the negative tip loading also rolls up in the analysis, with a core radius of 30% mean chord. To avoid having the rollup model respond to small regions of negative loading, the dual-peak model is only used at azimuths where the negative loading extends inboard at least to 0.945R (there are two aerodynamic panels outboard of this radial station). Two revolutions of wake are used, with calculated free distortion. There is partial entrainment of the trailed vorticity into the tip vortex, such that the final tip vortex strength (achieved after 1/4 revolution of wake age) is 70% of the peak bound circulation on the blade. The distorted wake geometry is calculated for the inboard vorticity as well as for the tip vortices, since inboard rollup is used in the negative tip loading areas. However, distortion of the inboard vorticity is not too important, except when drawing the wake geometry. These wake model features and parameters were determined based on the correlation with measured TRAM performance.

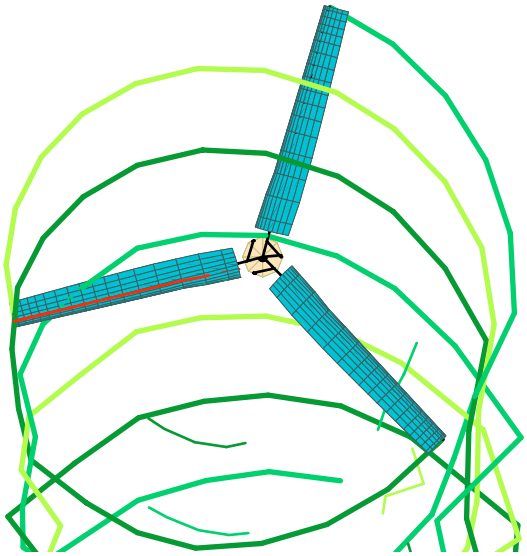

Figure 8. Calculated TRAM wake geometry for $\mu = 0.15$, $\alpha_s = 6$, $C_T/\sigma = 0.089$; blades at azimuth angles of 45, 165, 285 deg. Rolled-up wake model.

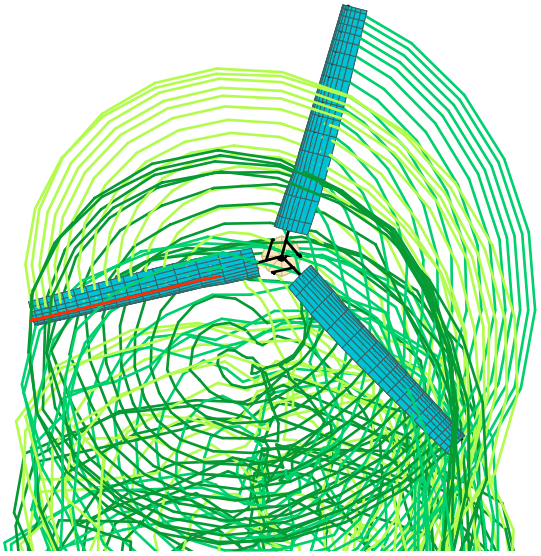

Figure 9. Calculated TRAM wake geometry for $\mu = 0.15$, $\alpha_s = 6$, $C_T/\sigma = 0.089$; blades at azimuth angles of 45, 165, 285 deg. Multiple-trailer wake model.

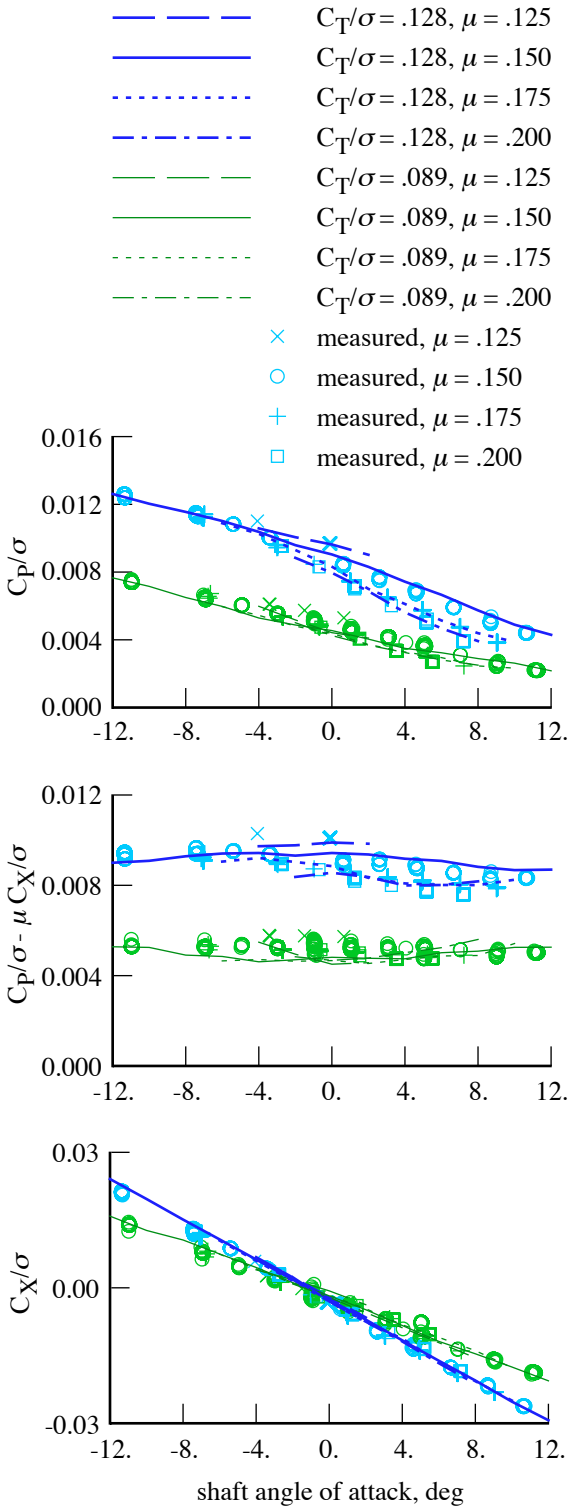

Figure 10. Measured and calculated TRAM helicopter mode performance. Rolled-up wake model.

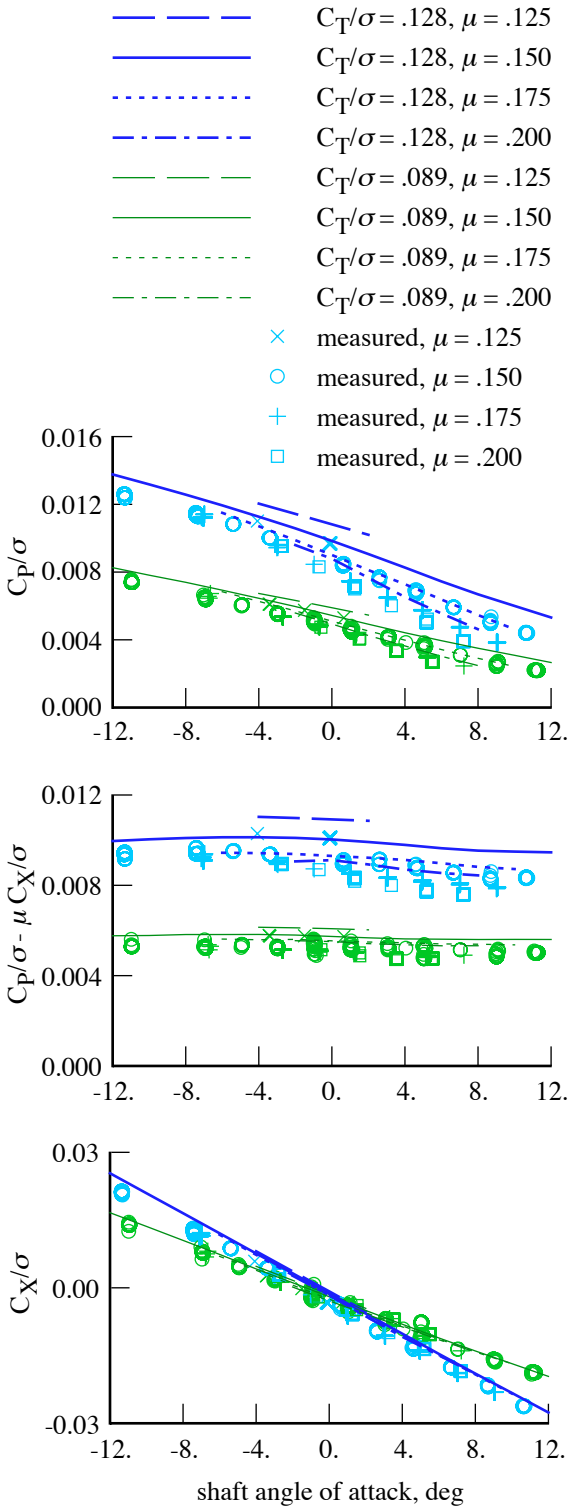

Figure 11. Measured and calculated TRAM helicopter mode performance. Multiple-trailer wake model.

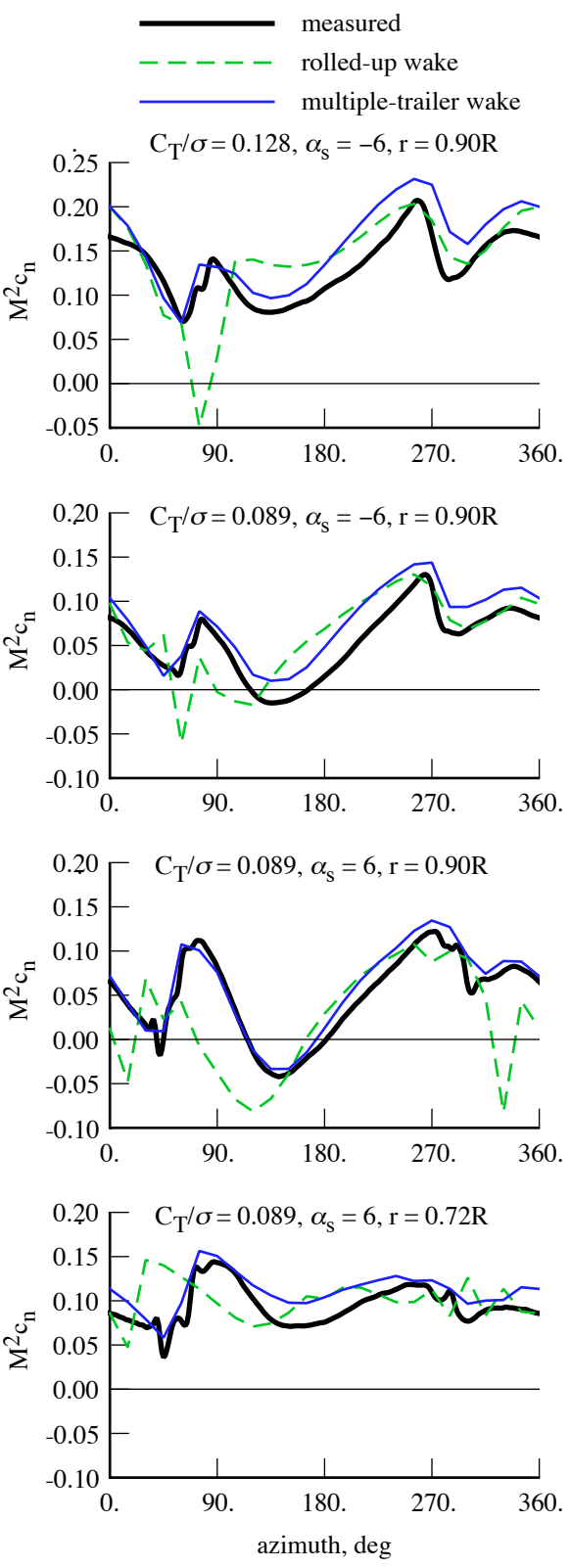

Figure 12. Measured and calculated TRAM helicopter mode airloads for $\mu = 0.15$.

There are major differences between this model and the corresponding aerodynamic and wake model that has been established for helicopter rotors (refs. 12 and 13). The primary differences are that the tiltrotor model includes the stall delay, does not use complete entrainment of the tip vortex, uses two revolutions of wake, and uses a restricted search for the circulation peak.

The multiple-trailer wake model (figure 9) has a discrete trailed vortex line emanating from each of the aerodynamic panel edges. The calculation of the free wake geometry in CAMRAD II includes the distortion of all of these trailed lines. Entrainment of the outboard lines into a tip vortex is evident in figure 9, but requires a substantial wake age to develop. Because of the low spanwise resolution and the absence of viscous effects, a highly concentrated tip vortex is not produced.

Performance and airloads calculated using the rolled-up and multiple-trailer wake models are compared with TRAM DNW measurements in reference 2. Figures 10 and 11 show the performance comparison for the two models. Performance calculated using the rolled-up wake model compares well with the measurements, although the induced power is probably too small for low thrust. The power calculated using the multiple-trailer wake model is significantly larger than measured and the propulsive force is larger, in contrast to the good correlation obtained using the rolled-up wake model. With the multiple-trailer wake model the calculated profile power is lower and the calculated induced power is significantly higher than with the rolled-up wake model.

Figure 12 compares the measured blade airloads (M^2c_n) with the calculations using the rolled-up and multiple-trailer wake models, at advance ratio $\mu = 0.15$, +6 and –6 deg shaft angle, and two radial stations. The results at other shaft angles and other radial stations are similar. The measured airloads and the airloads calculated using the multiple-trailer wake compare very well. The measured airloads integrate to a smaller rotor thrust, so the calculated airloads tend to have a larger mean value. The airloads calculated using the rolled-up wake model differ significantly from the measurements, particularly in the advancing side blade-vortex interactions. However, the wake geometry calculations with the multiple-trailer model do not produce a highly concentrated tip vortex. In contrast, measurements of the TRAM flow field show distinct rolled-up vortex structures, including both positive and negative vortices at low thrust (ref. 16). The vortices produce high-frequency oscillations in the measured airloads (figure 12), that this multiple-trailer wake model can never produce. The good airloads correlation using the multiple-trailer wake model implies that while the tiltrotor wake does roll up into concentrated vortices, the rollup process is occurring over a substantial wake age.

Thus the conclusion in reference 2 is that the rolled-up wake model gives the best correlation with performance measurements, while the multiple-trailer wake model is best for airloads calculations.

Wake Model With Consolidation

To improve the performance calculations for tiltrotors, while maintaining good airloads correlation, a recently developed free wake geometry method of CAMRAD II, which combines the multiple-trailer wake model with a simulation of the tip vortex formation process (ref. 9), is examined. This wake model is characterized as the multiple-trailer model with consolidation. Figures 13 and 14 illustrate the wake geometry for two forms of this model, compression and entrainment. The blades are at azimuth angles of 45, 165, and 285 deg; the operating condition is μ = 0.15, α_s = 6, C_T/σ = 0.089.

With multiple far wake trailed vorticity panels, the trailed lines at the wing panel edges can be consolidated into rolled-up lines, using the trailed vorticity moment to scale the rate of rollup. The rollup is not well calculated even with many trailed vortex lines, because of the coarse discretization and the neglect of viscosity. Hence it can be useful to impose consolidation in the wake geometry calculation. The consolidation model is intended for use with a trailed vortex line at each wing panel edge. The trailed vorticity is partitioned into sets of adjacent lines that have the same sign (bound circulation increasing or decreasing). It is assumed that all the vorticity in a set eventually rolls up into a single vortex, located at the centroid of the original vorticity distribution (refs. 17 and 18). For each set, the total strength G, centroid r_C, and moment (radius of gyration) r_G of the trailed vorticity in the set are calculated. Then the characteristic time (r_G^2/G) is taken as a measure of the rate of consolidation (refs. 19 and 20). The consolidation is implemented during the integration of the wake geometry, so the free wake geometry calculated is that of the consolidated wake.

The wing bound circulation Γ is calculated at the collocation points r_{Ak}, k = 1 to K. This bound circulation distribution produces trailed vorticity sheets with strength $-\partial\Gamma/\partial r$; discretized as vortex lines with strength $\delta_k = \Gamma_{k-1} - \Gamma_k$. The trailed vorticity is partitioned into sets of adjacent lines that have the same sign. The total strength G, centroid r_C, and moment (radius of gyration) r_G of the trailed vorticity in the set are:

$$G = \int (-\partial\Gamma/\partial r)\, dr$$

$$Gr_C = \int (-\partial\Gamma/\partial r)\, r\, dr$$

$$Gr_G^2 = \int (-\partial\Gamma/\partial r)\, (r-r_C)^2\, dr$$

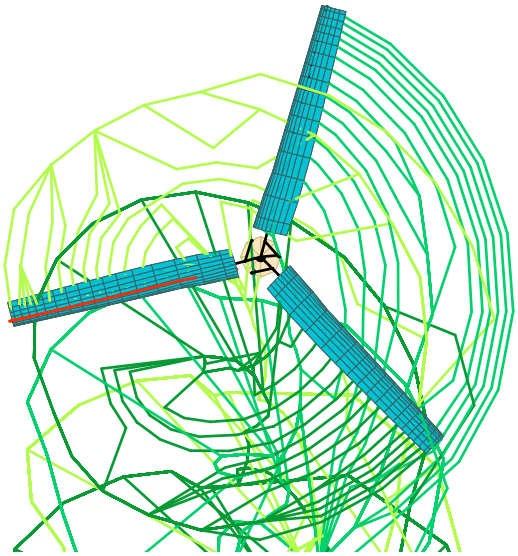

Figure 13. Calculated TRAM wake geometry for μ = 0.15, α_s = 6, C_T/σ = 0.089; blades at azimuth angles of 45, 165, 285 deg. Multiple-trailer wake model with consolidation, entrainment form.

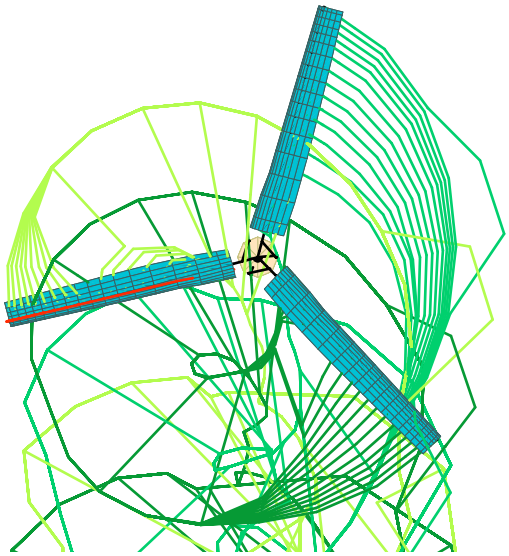

Figure 14. Calculated TRAM wake geometry for μ = 0.15, α_s = 6, C_T/σ = 0.089; blades at azimuth angles of 45, 165, 285 deg. Multiple-trailer wake model with consolidation, compression form.

For trailed vortex elements at wake age τ, the total strength and moment are evaluated at the time the vorticity was created ($t-\tau$), and used to calculate the time constant $\tau_{cons} = k_{cons}(r_G{}^2/G)$. Then the fraction of rollup, f_{cons}, is evaluated using an exponential (ref. 19), linear, or power dependence on wake age:

$$f_{cons} = 1 - \exp(-(\tau-\tau_B)/\tau_{cons}) \quad \text{exponential}$$
$$= (\tau-\tau_B)/\tau_{cons} \quad \text{linear}$$
$$= ((\tau-\tau_B)/\tau_{cons})^m \quad \text{power}$$

The consolidation starts at wake age τ_B. In addition, a maximum consolidation fraction $f_E \le 1$ can be specified. For all the results presented in this paper, the linear dependence of the rollup fraction with wake age is used; with $\tau_B = 0$ and $f_E = 1$.

The consolidation can be accomplished by entrainment or by compression. With the entrainment form, vortex lines are consolidated into a single line of strength $f_{cons}G$. For the k-th trailed vorticity line, originating from the panel edge at r_{Ek}, f_k is the fraction of the vorticity in the set that is within the distance $|r_{Ek}-r_C|$ from the centroid. Then the vortex lines in the set that are consolidated at age τ are those for which $f_k \le f_{cons}$ (all lines within the minimum $|r_{Ek}-r_C|$ such that the strength is $f_{cons}G$). The consolidation is implemented by replacing the position of each consolidated line with the position of the centroid: $r_{cons} = \Sigma\delta_k r_{Wk}/\Sigma\delta_k$; where r_{Wk} is the position and δ_k is the strength of the k-th trailed vortex line, and the sums are over the consolidated lines in the set. Figure 13 illustrates the wake geometry obtained using the entrainment form.

With the compression form, f_{cons} is the fraction of consolidation. If $f_{cons} \ge 1$, the position of each line is replaced with the position of the centroid: $r_{cons} = \Sigma\delta_k r_{Wk}/\Sigma\delta_k$; where the sums are over all the lines in the set. If $f_{cons} < 1$, the position of each line is replaced with $(1-f_{cons})r_{Wk} + f_{cons}r_{cons}$. Figure 14 illustrates the wake geometry obtained using the compression form.

In addition, the wake models of CAMRAD II allow the vortex core radius to be defined in several ways (ref. 9). The vortex core radius is specified by a constant term (input fraction of chord, r_{c0}/c); a term growing with wake age τ (using an input exponent n, and τ_1 = wake age for core radius of 100% chord); and a term that scales with the trailed vorticity moment. Hence the general expression for the core radius is:

$$r_c = c\,(r_{c0}/c) + c\,(\tau/\tau_1)^n + f_M\, r_G$$

where r_G is the second moment about the centroid (the radius of gyration) of the trailed vorticity, evaluated at the time the vortex element was created. This moment is obtained by integrating the vorticity for all adjacent trailed lines of the

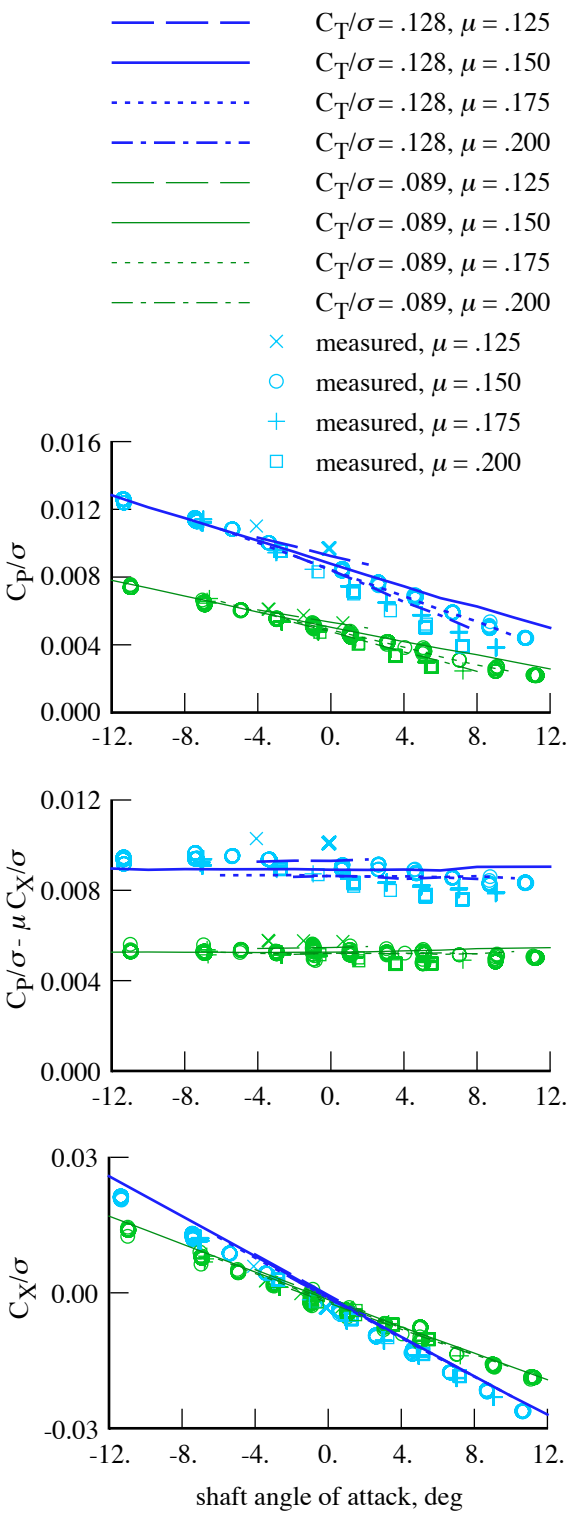

Figure 15. Measured and calculated TRAM helicopter mode performance. Multiple-trailer wake model with consolidation (compression form).

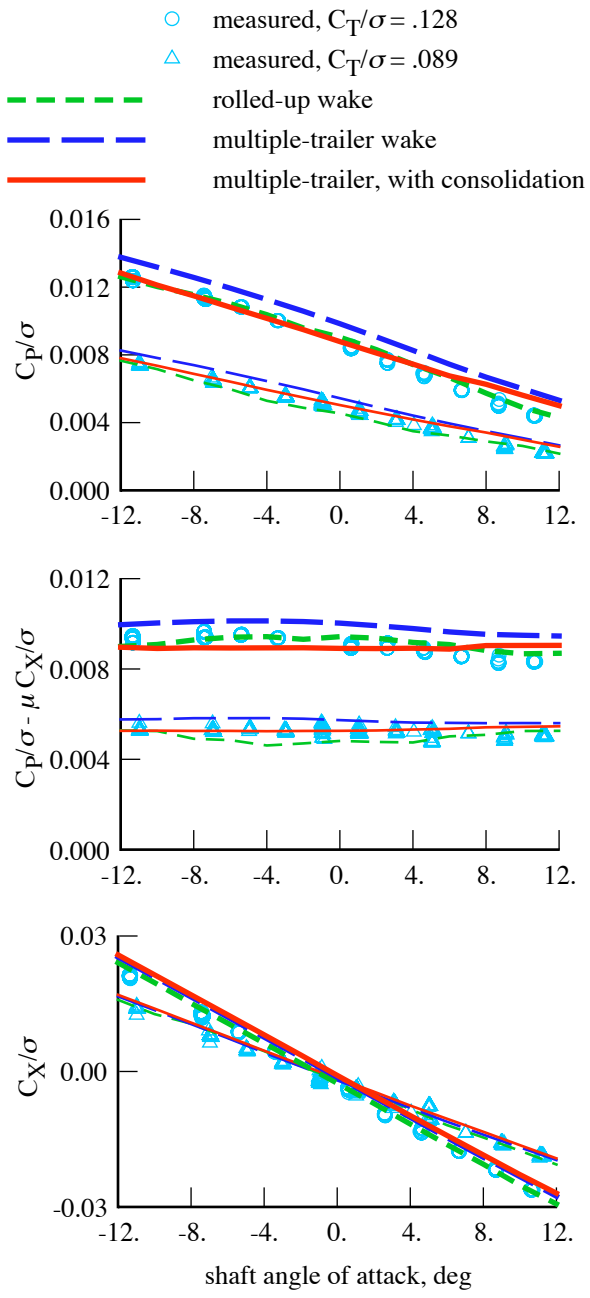

Figure 16a. Influence of wake model on calculated TRAM helicopter mode performance ($\mu = 0.15$; heavy line $C_T/\sigma = 0.128$, thin line $C_T/\sigma = 0.089$; compression form for consolidation).

same sign. Equating the moment of the trailed vorticity created behind the blade to the moment of the rolled up vortex implies that the constant f_M should be on the order of 1.0 (depending on the vorticity distribution in the vortex core).

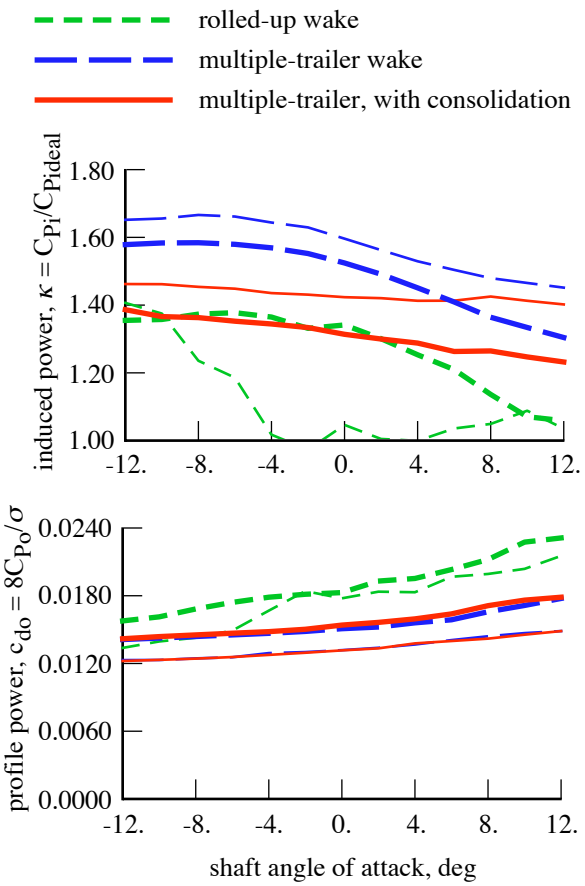

Figure 16b. Influence of wake model on calculated TRAM helicopter mode performance ($\mu = 0.15$; heavy line $C_T/\sigma = 0.128$, thin line $C_T/\sigma = 0.089$; compression form for consolidation).

Results

The TRAM helicopter mode performance calculated using the multiple-trailer wake model with consolidation is shown in figure 15. The consolidation model uses the compression form, with linear dependence of the rollup fraction on wake age: $f_{cons} = \tau/\tau_{cons}$ with $\tau_{cons} = 5(r_G^2/G)$ ($k_{cons} = 5$). The vortex core radius has a constant value of 80% mean chord ($r_c = 0.8c$). The power calculation is much improved compared to the results without consolidation (figure 11), although not quite as good as the results from the rolled-up wake model (figure 10).

The influence of the wake model on the calculated TRAM helicopter mode performance for $\mu = 0.15$ is examined in figure 16. The power calculated using the multiple-trailer wake model is too high. Using the multiple-trailer model with consolidation, the power correlation is good, although the calculated power is somewhat high at large (aft) shaft angles. The calculated propulsive force is not

very sensitive to the wake model, but the propulsive force is somewhat high using the multiple-trailer models. The calculated propulsive force matches the data well, so the differences between measurement and calculation are similar for power and equivalent drag. At low thrust, the induced power calculated using the rolled-up wake model is too low; a ratio of induced power to ideal power that is close to 1.0 is not likely. With the multiple-trailer models, the induced power is higher and the profile power lower than with the rolled-up wake model. Using consolidation in the multiple-trailer model lowers the calculated induced power, so the correlation with measured power is improved.

Figure 17 shows the corresponding comparison of measured and calculated airloads. The correlation using consolidation is not quite as good as for the multiple-trailer wake model without consolidation, but still a substantial improvement compared to the results of the rolled-up wake model. Consequently, by using the multiple-trailer wake model with consolidation, good correlation of the calculations with TRAM measurements is obtained for both performance (figure 15) and for airloads (figure 17).

The compression and entrainment forms of the wake geometry consolidation model (figures 13 and 14) produce nearly the same results for performance and low frequency airloads. Figure 18 compares the induced power calculated using the two forms, and figure 19 shows the calculated and measured airloads. No effect was found on performance or airloads using a faster consolidation rate, $k_{cons} = 1$ instead of the baseline value of 5.

The calculations from the consolidation model that have been presented in figures 16 to 19 are for a vortex core radius with a constant value of 80% mean chord ($r_c = 0.8c$). The core radius has a small influence on calculated performance, and some influence on the calculated airloads. Figure 20 compares the induced power calculated using a constant core radius of 80% and 40% mean chord, and a core radius proportional to the trailed vorticity moment ($r_c = 1.5r_G$). Figure 21 shows the corresponding calculated airloads, including $r_c = 1.0r_G$ and $2.0r_G$ results. The airloads are nearly the same for $r_c = 0.8c$ and $r_c = 1.0r_G$, while $r_c = 2.0r_G$ reduces the blade-vortex interaction loads, particularly on the advancing side.

Finally, figure 22 shows the airloads calculated using an azimuthal resolution of 3 deg (instead of 15 deg as in figure 17), for the multiple-trailer wake model and the multiple-trailer model with consolidation. These high resolution results are produced by first obtaining the equilibrium solution of the coupled aerodynamic, wake, structural, and inertial problem at 15 deg azimuthal resolution, and then evaluating the airloads at 3 deg resolution using the blade motion from the 15 deg solution. With consolidation, the high resolution solution does exhibit high frequency blade-

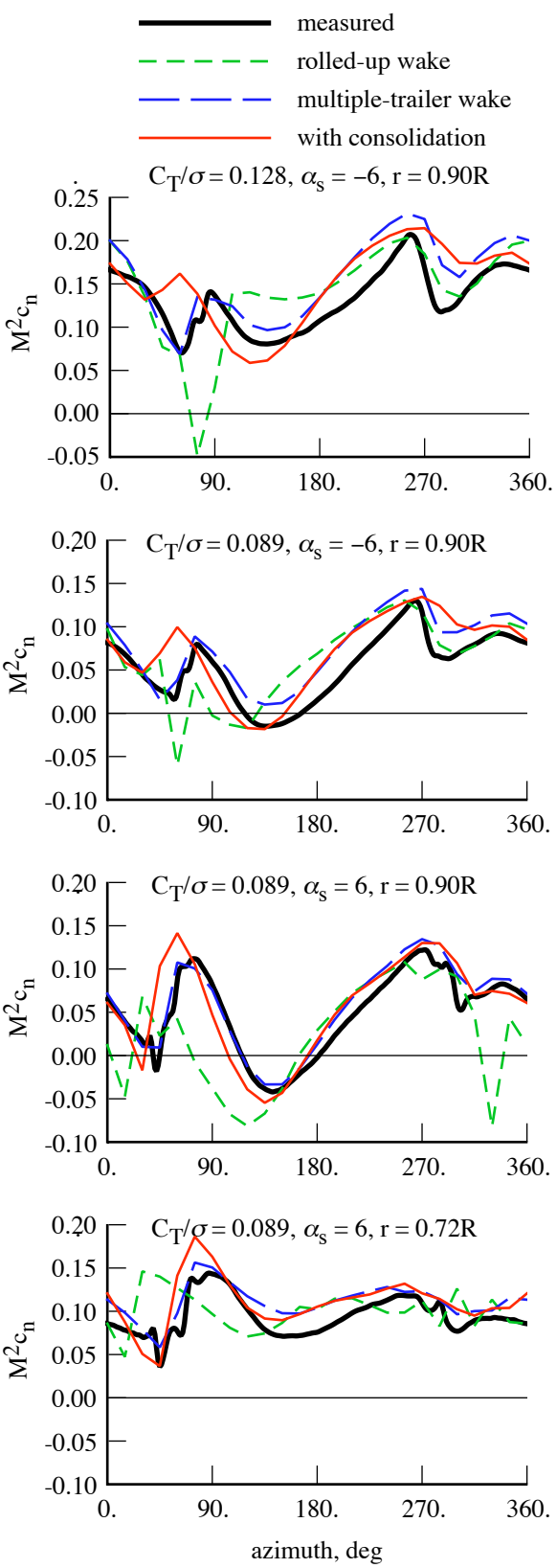

Figure 17. Influence of wake model on calculated TRAM helicopter mode airloads ($\mu = 0.15$).

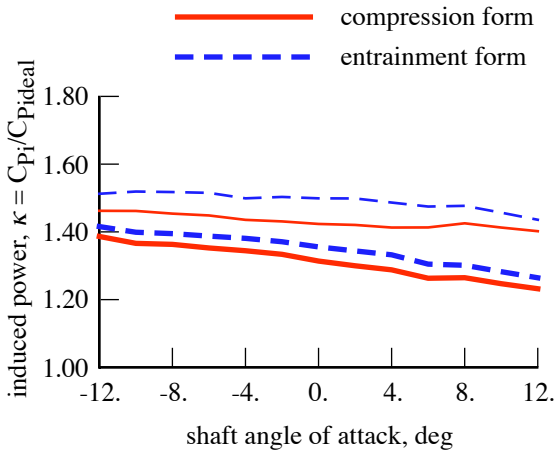

Figure 18. Influence of wake model on calculated TRAM helicopter mode performance ($\mu = 0.15$; heavy line $C_T/\sigma = 0.128$, thin line $C_T/\sigma = 0.089$). Multiple-trailer wake model with consolidation; compression and entrainment forms.

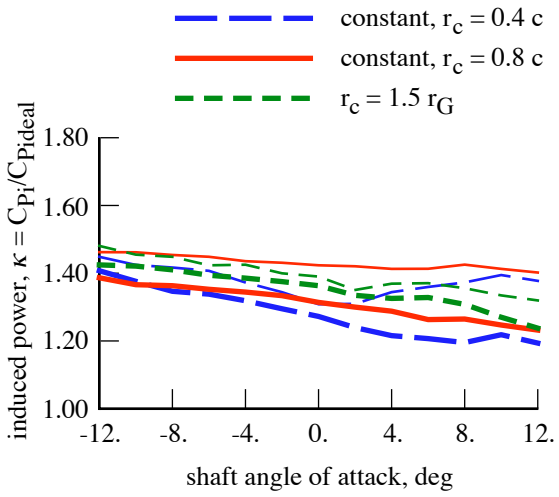

Figure 20. Influence of vortex core radius on calculated TRAM helicopter mode performance ($\mu = 0.15$; heavy line $C_T/\sigma = 0.128$, thin line $C_T/\sigma = 0.089$). Multiple-trailer wake model with consolidation.

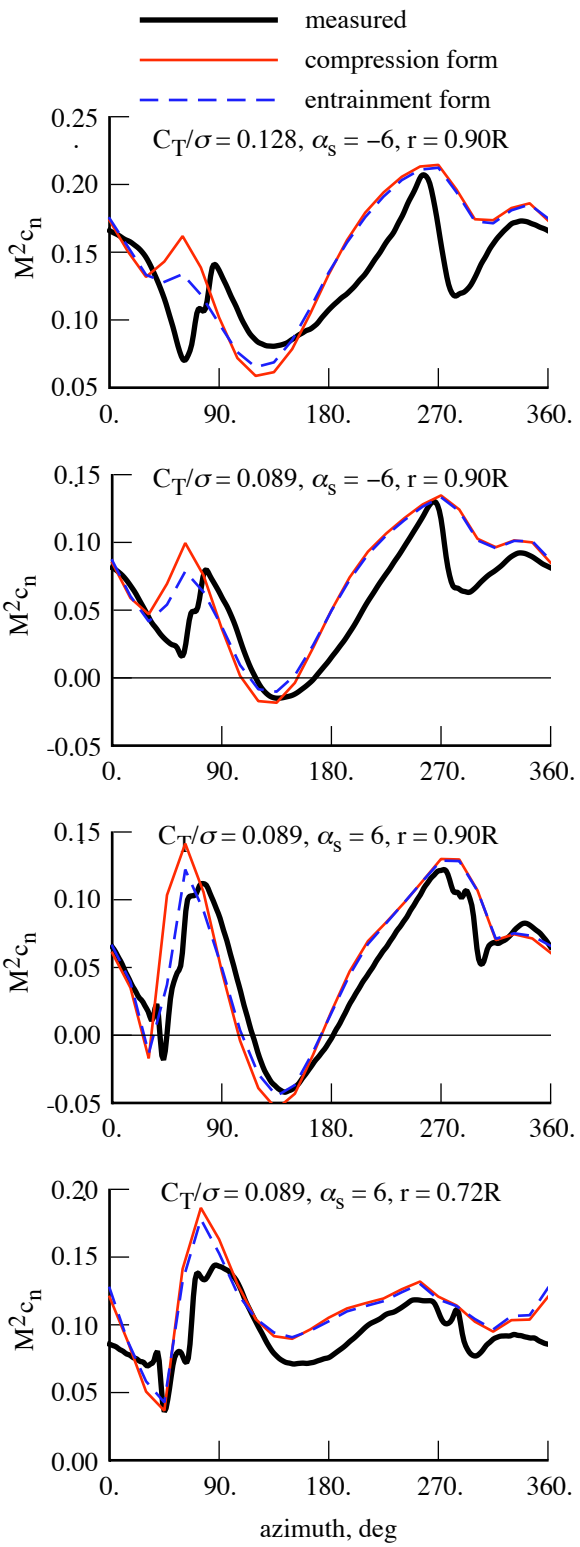

Figure 19. Influence of wake model on calculated TRAM helicopter mode airloads ($\mu = 0.15$). Multiple-trailer wake model with consolidation; compression and entrainment forms.

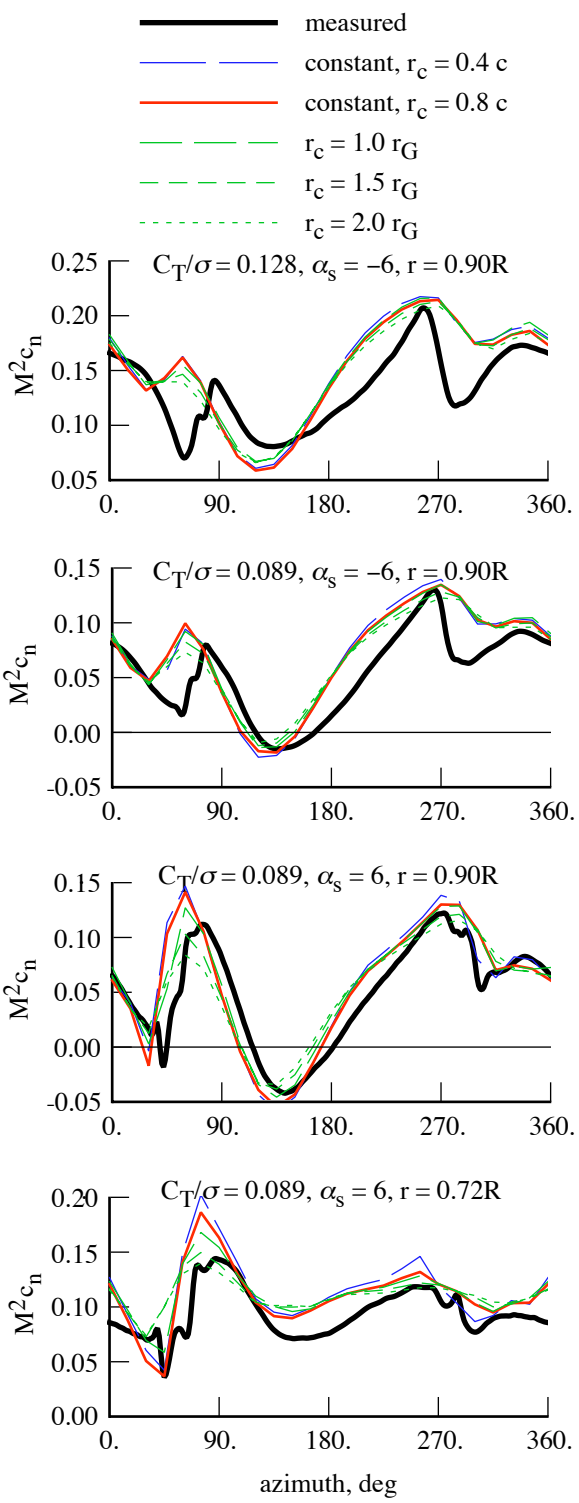

Figure 21. Influence of vortex core radius on calculated TRAM helicopter mode airloads (μ = 0.15). Multiple-trailer wake model with consolidation.

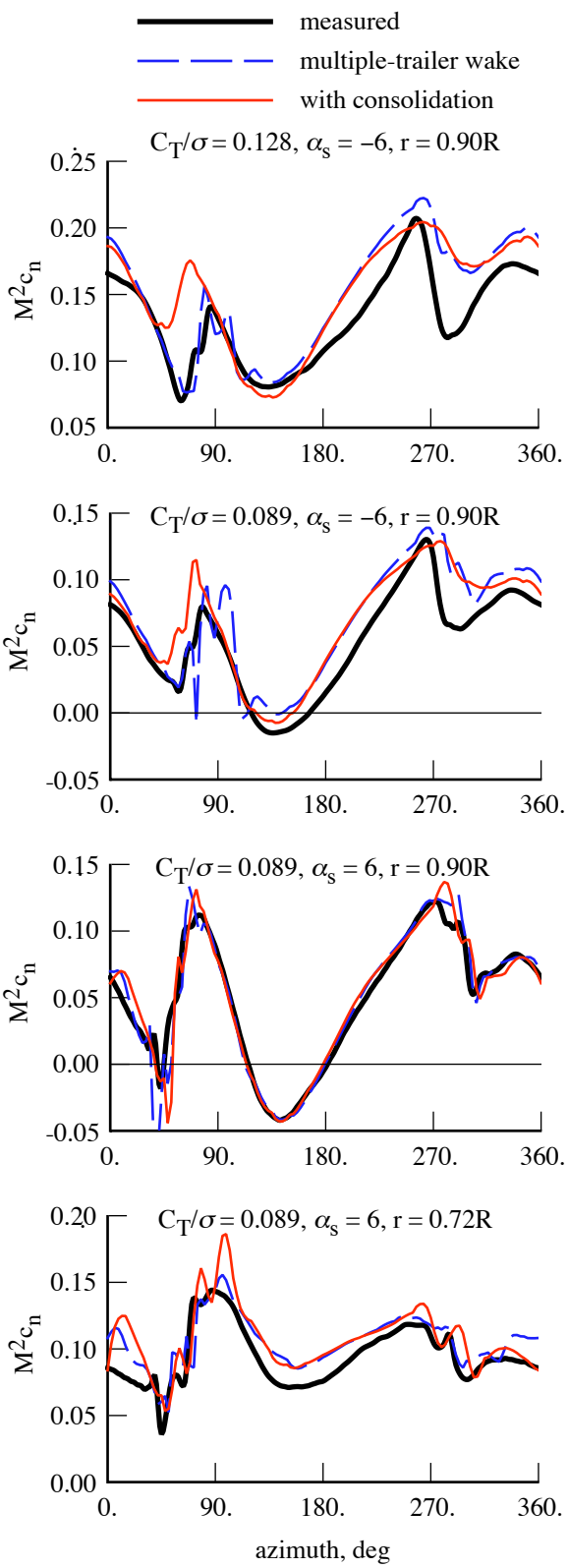

Figure 22. Influence of wake model on calculated TRAM helicopter mode airloads (μ = 0.15). High resolution calculation (azimuth increment 3 deg).

vortex interactions similar to those in the measured airloads. Without consolidation, the multiple-trailer wake model produces spurious blade-vortex interactions, associated with the individual trailed vortex lines.

Concluding Remarks

Comparisons of measured and calculated aerodynamic behavior of a tiltrotor model have been presented. The measured data are from the test of the Tilt Rotor Aeroacoustic Model (TRAM) with a single, 1/4-scale V-22 rotor in the German-Dutch Wind Tunnel (DNW). The calculations were performed using the rotorcraft comprehensive analysis CAMRAD II.

The focus of this paper has been the further development of wake models for tiltrotors in helicopter mode operation. Three tiltrotor wake models are considered, characterized as the rolled-up, multiple-trailer, and multiple-trailer with consolidation models.

The rolled-up wake model for tiltrotors evolved from the typical helicopter wake model, and features a fully developed tip vortex (and an inboard vortex when there is negative loading of the blade tip). A major difference between this model and the corresponding wake model that has been established for helicopter rotors is that the tiltrotor model does not use complete entrainment of the tip vortex. The multiple-trailer wake model has a discrete trailed vortex line emanating from each of the wing aerodynamic panel edges. The calculation of the free wake geometry includes the distortion of all trailed lines, but because of the low spanwise resolution and the absence of viscous effects, a highly concentrated tip vortex is not produced. Good performance correlation is achieved using the rolled-up wake model, but the calculated airloads are not accurate. Good airloads correlation is achieved using the multiple-trailer wake model, but the calculated power is too large.

By using the free wake geometry calculation method of CAMRAD II that combines the multiple-trailer wake model with a simulation of the tip vortex formation process (consolidation), good correlation of the calculations with TRAM measurements is obtained for both performance and airloads. With the consolidation model, the trailed lines at the wing panel edges are combined into rolled-up vortices, using the trailed vorticity moment to scale the rate of rollup. All the vorticity in adjacent lines that have the same sign (bound circulation increasing or decreasing) eventually rolls up into a single vortex, located at the centroid of the original vorticity distribution. For performance and airloads calculations, nearly the same results are obtained using the compression form and the entrainment form of the consolidation model.

Two aspects of the analysis that clearly need improvement are the stall delay model and the trailed vortex formation model. These features represent specific physical aspects of rotor aerodynamics, that are described directly, but quite simply, in the aerodynamic and wake model of the analysis. One result of the correlation is to establish values of the parameters that define these features in CAMRAD II. The more general results of the correlation are to establish the key importance of these features for tiltrotor aeromechanics behavior, and the need for improved models. A first-principles solution for rotor aerodynamics is the long term goal. Until that is available, more accurate and more general models of the stall delay and the trailed vortex formation are needed. Acquisition of additional detailed aerodynamic measurements will be needed to support such model development.

Although the tiltrotor model developed in this investigation is considered generic, these calculations must be repeated for other tiltrotor configurations in order to establish the generality of the models. A candidate for additional comparison between measured and calculated tiltrotor aeromechanics behavior is the helicopter mode test of an isolated, full-scale XV-15 rotor in the Ames Research Center 80- by 120-Foot Wind Tunnel.

References

1) Johnson, W. "Calculation of Tilt Rotor Aeroacoustic Model (TRAM DNW) Performance, Airloads, and Structural Loads." American Helicopter Society Aeromechanics Specialists' Meeting, Atlanta, Georgia, November 2000.

2) Johnson, W. "Calculation of the Aerodynamic Behavior of the Tilt Rotor Aeroacoustic Model (TRAM) in the DNW." American Helicopter Society 57th Annual Forum Proceedings, Washington, D.C., May 2001.

3) Young, L.A. "Tilt Rotor Aeroacoustic Model (TRAM): A New Rotorcraft Research Facility." Heli Japan 98: AHS International Meeting on Advanced Rotorcraft Technology and Disaster Relief, April 1998, Nagarafukumitsu, Gifu, Japan.

4) Young, L.A.; Booth, E.R., Jr.; Yamauchi, G.K.; Botha, G.; and Dawson, S. "Overview of the Testing of a Small–Scale Proprotor." AHS International 55th Annual Forum Proceedings, Montreal, Canada, May 1999.

5) Swanson, S.M.; McCluer, M.S.; Yamauchi, G.K.; and Swanson, A.A. "Airloads Measurements from a 1/4–Scale Tiltrotor Wind Tunnel Test." 25th European Rotorcraft Forum, Rome, Italy, September 1999.

6) Johnson, J.L., and Young, L.A. "Tilt Rotor Aeroacoustic Model Project." Confederation of European Aerospace Societies (CEAS), Forum on Aeroacoustics of Rotorcraft and Propellers, Rome, Italy, June 1999.

7) Ames Research Center. "TRAM Physical Description." NASA Report (to be published).

8) Jenks, M.D., and Narramore, J.C. "Final Report for the 2–D Test of the Model 901 Rotor and Wing Airfoils (BSWT 592)," Boeing Report D901–99065–1, June 1984.

9) Johnson, W. "CAMRAD II, Comprehensive Analytical Model of Rotorcraft Aerodynamics and Dynamics." Johnson Aeronautics, Palo Alto, California, 1992–2002.

10) Johnson, W. "Technology Drivers in the Development of CAMRAD II." American Helicopter Society Aeromechanics Specialists Conference, San Francisco, California, January 1994.

11) Johnson, W. "Rotorcraft Aeromechanics Applications of a Comprehensive Analysis." Heli Japan 98: AHS International Meeting on Advanced Rotorcraft Technology and Disaster Relief, April 1998.

12) Johnson, W. "A General Free Wake Geometry Calculation for Wings and Rotors." American Helicopter Society 51st Annual Forum Proceedings, Fort Worth, Texas, May 1995.

13) Johnson, W. "Rotorcraft Aerodynamics Models for a Comprehensive Analysis." AHS International 54th Annual Forum Proceedings, Washington, D.C., May 1998.

14) Corrigan, J.J., and Schillings, J.J. "Empirical Model for Stall Delay Due to Rotation." American Helicopter Society Aeromechanics Specialists Conference, San Francisco, California, January 1994.

15) Du, Z., and Selig, M.S. "A 3–D Stall–Delay Model for Horizontal Axis Wind Turbine Performance Prediction." AIAA Paper 98–0021, January 1998.

16) Yamauchi, G.K.; Burley, C.L.; Mercker, E.; Pengel, K; and JanakiRam, R. "Flow Measurements of an Isolated Model Tilt Rotor." AHS International 55th Annual Forum Proceedings, Montreal, Canada, May 1999.

17) Betz, A. "Behavior of Vortex Systems." Zeitschrift fuer Angewandte, Mathematik und Mechanik, Bd. XII, Nr. 3, 1932; also NACA TM 713, 1933.

18) Rossow, V.J. "On the Inviscid Rolled-Up Structure of Lift-Generated vortices." Journal of Aircraft, Volume 10, Number 11, November 1973.

19) Bilanin, A.J., and Donaldson, C.DuP. "Estimation of Velocities and Roll-Up in Aircraft Vortex Wakes." Journal of Aircraft, Volume 12, Number 7, July 1975.

20) Quackenbush, T.R.; Lam, C.-M.G.; Wachspress, D.A.; and Bliss, D.B. "Computational Analysis of High Resolution Unsteady Airloads for Rotor Aeroacoustics." NASA CR 194894, May 1994.

Table 2. Measured operating condition of helicopter mode points selected for detailed examination.

$V/\Omega R$ = 0.15, C_T/σ = 0.089						
nominal shaft angle	–10	–6	–2	2	6	10
run	607	605	605	605	603	603
point	13	231	122	10	7	72
advance ratio, $V/\Omega R$	.1509	.1506	.1509	.1502	.1495	.1506
rotor thrust, C_T/σ	.08814	.08792	.08831	.08895	.08839	.08949
shaft angle of attack	–9.99	–6.00	–2.03	1.99	5.94	9.95
corrected shaft angle of attack	–10.92	–6.94	–2.97	1.04	4.98	9.02
tip Mach number, M_{tip}	.6278	.6248	.6259	.6281	.6294	.6271
air density, ρ	.002334	.002326	.002336	.002354	.002373	.002356
air temperature (deg F)	59.69	64.37	62.62	59.20	57.98	61.55
azimuth correction, $\Delta\psi$	1.48	1.30	1.11	.94	.75	.53
rotor power, C_P/σ	.007386	.006516	.005567	.004656	.003683	.002603
rotor propulsive force, C_X/σ	.01382	.00809	.00191	–.00480	–.01091	–.01628
longitudinal gimbal tilt, β_{1c}	–.04	.07	.09	.03	–.14	–.30
lateral gimbal tilt, β_{1s}	–.08	–.09	.16	.10	–.13	–.33
C_T/σ from pressures	.0661	.0731	.0712	.0702	.0795	.0809
missing c_n	.96R				.82 R	.82 R
missing flap moment	.365 R	.365 R	.365 R	.365 R	.365 R	.365 R
missing torsion moment	.76 R	.76 R				
$V/\Omega R$ = 0.15, C_T/σ = 0.128						
nominal shaft angle	–10	–6	–2	2	6	10
run	607	605	605	605	603	603
point	68	252	177	68	13	39
advance ratio, $V/\Omega R$	.1506	.1503	.1500	.1512	.1504	.1501
rotor thrust, C_T/σ	.12679	.12619	.12371	.12665	.12662	.12625
shaft angle of attack	–9.98	–5.99	–2.10	1.93	5.95	10.03
corrected shaft angle of attack	–11.32	–7.34	–3.43	.59	4.60	8.69
tip Mach number, M_{tip}	.6264	.6247	.6254	.6266	.6290	.6280
air density, ρ	.002325	.002325	.002330	.002342	.002369	.002361
air temperature (deg F)	61.89	64.64	63.72	61.67	58.90	60.57
azimuth correction, $\Delta\psi$	2.47	2.25	1.92	1.69	1.37	1.02
rotor power, C_P/σ	.012392	.011290	.009617	.008402	.006704	.005002
rotor propulsive force, C_X/σ	.02137	.01239	.00455	–.00377	–.01364	–.02190
longitudinal gimbal tilt, β_{1c}	.06	.26	.09	.10	.22	.23
lateral gimbal tilt, β_{1s}	–.03	.01	.00	.09	.31	.26
C_T/σ from pressures	.0986	.1084	.1045	.1050	.1145	.1136
missing c_n	.96R				.82 R	.82 R
missing flap moment	.365 R	.365 R	.365 R	.365 R	.365 R	.365 R
missing torsion moment	.76 R	.76 R				